Editors' Suggestion | Featured in Physics

Guiding Self-Assembly of Active Colloids by Temporal Modulation of Activity

Bo Zhang, Alexey Snezhko, and Andrey Sokolov*
Materials Science Division, Argonne National Laboratory, 9700 South Cass Avenue, Lemont, Illinois 60439, USA

(Received 10 August 2021; accepted 17 December 2021; published 7 January 2022)

Self-organization phenomena in ensembles of self-propelled particles open pathways to the synthesis of new dynamic states not accessible by traditional equilibrium processes. The challenge is to develop a set of principles that facilitate the control and manipulation of emergent active states. Here, we report that dielectric rolling colloids energized by a pulsating electric field self-organize into alternating square lattices with a lattice constant controlled by the parameters of the field. We combine experiments and simulations to examine spatiotemporal properties of the emergent collective patterns and investigate the underlying dynamics of the self-organization.We reveal the resistance of the dynamic lattices to compression and expansion stresses leading to a hysteretic behavior of the lattice constant. The general mechanism of pattern synthesis and control in active ensembles via temporal modulation of activity can be applied to other active colloidal systems.

DOI: 10.1103/PhysRevLett.128.018004

The subject of vast interest in the field of active matter physics is the emergence of self-organized collective behavior out of chaotic motions of individual particles as a result of interparticle interactions [1–7]. Self-organization phenomena in biological active systems, such as flocks of birds and schools of fish, rely on communications, visual monitoring, and sensing of individual positions and requires constant brain processing of collected information [8–11]. A collective motion in ensembles of simple organisms, such as swimming bacteria, may arise only out of interparticle steric and hydrodynamic interactions [12–18], which makes them a popular model system for the investigation of collective behaviors and self-organization phenomena.

Systems of synthetic self-propelled particles, energized by chemical reactions or electromagnetic fields, provide even better control over individual and collective dynamics of active units and, as a result, complex out-of-equilibrium dynamics of such systems is the subject of extensive research [5,6,19–26]. Currently, the majority of collective phenomena are observed in the systems with a constant (or nearly constant) energy injection rate. For instance, a system of electrostatically driven rolling colloids, Quincke rollers, exhibits a large variety of dynamic phases ranging from an isotropic gas to polar bands, vortices, swarms, and rotating clusters [5,19,27,28]. The temporal modulation of activity in that system was recently suggested to model behavior of living systems and control clustering of particles [6,29,30].

In this Letter, we report self-assembly of active Quincke rollers into dynamic square lattices when energized by a spatially uniform but modulated in time electric field. The formation of dynamic structures is triggered by a momentarily decoupling between dominant interparticle interactions–hydrodynamic velocity alignment and near-field electrostatic repulsion as a result of a temporal cessation of the energy injection. Temporal cessation of the activity resets particles' interactions and redirects velocities according to the locally formed particle arrangements. In contrast to vertically vibrated granular matter [31–34], only square lattices are observed, and these lattices preserve their structure after termination of the activity.

In our experiments, spherical polystyrene particles of the diameter $d = 4.8\ \mu$m are dispersed in 0.15 mol L^{-1} AOT-hexadecane solution and sandwiched between two parallel ITO-coated glass slides spaced 45 μm apart, see Fig. 1(a). When a static (dc) electric field is applied, particles polarize, and above the critical amplitude of the field [19] they start to steadily rotate and roll on the bottom surface with a constant speed driven by electrohydrodynamic Quincke rotation phenomenon [35,36]. The typical velocity of rollers in our experiments is 0.8 mm/s. At a particle area fraction above $\phi_c \approx 0.002$, rollers form a steady vortex or a traveling band in confined systems [19,27,37]. The temporal profile of the mean square displacement (MSD) for individual rollers [red curve in Fig. 1(d)] reveals long ballistic regime of motion.

The behavior of rollers becomes drastically different if activity of particles is modulated by the pulsating electric field shown in Fig. 1(b). For simplicity, we fix the magnitude of the electric field, but probe the rollers' dynamics by varying only the duration of pulses τ_{on} and the interval between the pulses τ_{off}. This technique was recently suggested to model run-and-tumble behavior and Lévy walks via incomplete depolarization of rollers at relatively short resting time τ_{off} [6]. The formation of lattices observed in our work requires full depolarization of

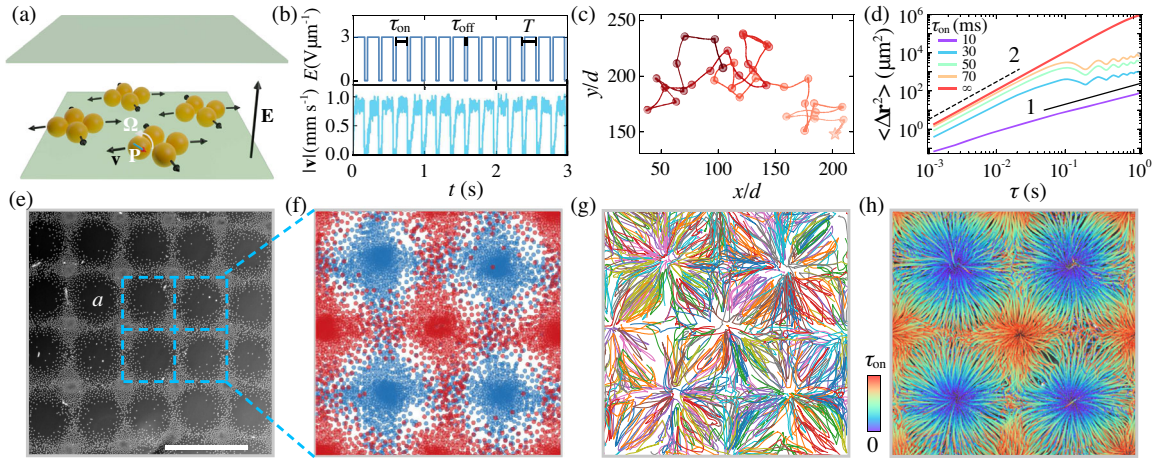

FIG. 1. Self-assembly of Quincke rollers into square lattices under a pulsating electric field. (a) A sketch of the experimental setup. (b) Temporal dependence of the electric field and the averaged particles' velocity. $T = \tau_{on} + \tau_{off}$ is the period of the signal. (c) A trajectory of an isolated roller energized by the pulsating electric field. (d) Mean square displacement curves of the rollers under periodic activity modulations. The bottom (purple) and the top (red) curves correspond to the motion of the rollers in gas and vortex phases, respectively. $E = 2.7\ \mathrm{V}\,\mu\mathrm{m}^{-1}$ and $T = 100$ ms for all curves except the case of a constant field. Slopes marked as 1 and 2 indicate diffusive ($\sim\tau$) and ballistic ($\sim\tau^2$) regimes, respectively. (e) An experimental snapshot of a dynamic square lattice captured between electric field pulses. The blue squares marks four unit cells with a lattices constant a. The same area is also shown in (f)–(h). The particle area fraction $\phi = 0.114$, $E = 3.0\ \mathrm{V}\,\mu\mathrm{m}^{-1}$, $T = 125$ ms, $\tau_{on} = 112.5$ ms. The scale bar is 0.5 mm. See also Supplemental Material, Video S1 [38]. (f) Overlayed square lattices formed after two consecutive cycles represented by blue and red circles. (g) Visualization of the particle trajectories over five periods of the field. For clarity only 10% of particle trajectories are shown. (h) Color-coded visualization of the time evolution of particles positions during one cycle. The color in each point of a particle trajectory corresponds to the time between zero (purple) and τ_{on} (red) as shown by the color bar.

particles after each cycle of the electric field, which occurs if τ_{off} is several times larger than the Maxwell-Wagner polarization relaxation time τ_{MW} [$\tau_{MW} = (\epsilon_p + 2\epsilon_f)/(\sigma_p + 2\sigma_f) \approx 1$ ms], where $\epsilon_{p,f}$ and $\sigma_{p,f}$ are the permittivities and conductivities of particles (p) and fluids (f), respectively. Relaxation of large-scale flows and hydrodynamic interactions occur within viscous timescale that in the experimental cell of the thickness $d = 45$ μm is on the order of 1 ms. As a result, each roller in our experiments comes to a complete rest for $\tau_{off} > 10$ ms. The Brownian motion has a negligible effect on particles' motion due to their large size and does not alter their positions when activity is terminated. At low concentrations ($\phi < \phi_c$), each particle randomizes the velocity direction in each period [Fig. 1(c) and Supplemental Material [38], Fig. S9].

At a high particle concentration, the initial direction of motion upon field application is affected by an arrangement of neighbors. Rollers tend to move against the local gradient of particle density due to the electrostatic repulsion between polarized particles [30]. The spontaneous formation of a cluster is followed by its quick explosive decay and concentration of particles in previously depleted areas during the next cycle. While initially the positions of nuclei clusters are random, they slowly evolve into a well-defined stable structure, and in several hundred activity cycles, particles' positions start to alternate between two sets of nearly perfect square lattices (**A** and **B**) with the same lattice constant a, see Figs. 1(e) and 1(f) and Supplemental Material, Fig. S1 and Video S1 [38]. The structures of lattices **A** and **B** are geometrically identical but translated by the half of a diagonal of the unit cell $(a/2, a/2)$. A closer inspection of particles' motion shows that the average distance particles travel each cycle is noticeably smaller than the shift between the lattices ($\sqrt{2}a/2$), see Figs. 1(g) and 1(h). The particles preserve their positions in one of two lattices as long as the field is off, but quickly form the alternative lattice upon the next pulse of the electric field. Therefore, the observed self-organization of particles is intrinsically different from activity-induced cluster formation in which active particles slow down in crowded areas, further increasing the local density and the size of the cluster. [3,39,40]. The reciprocating motion of rollers between the two lattices (period is $2T$) effectively traps individual particles within unit cells for several cycles, as reflected by the oscillation of MSD curves and particle trajectories [Figs. 1(d) and 1(g)]. The motion of particles eventually becomes diffusive as particles migrate from cell to cell over the system. The diffusion constant D increases with particle run time τ_{on}, see Fig. S3(a) in [38].

Our minimalistic phenomenological model (see [38] for details), which involves only isotropic interparticle repulsion and velocity alignment mechanisms, accurately reproduces the formation of patterns observed in experiments (see Figs. S2 and S3 in [38]), as well as main dynamic properties of the lattices discussed below. The results of our simulations highlight the role of repulsive forces

immediately upon the system activation. In the model, while the system is active, all particles move with nearly the same constant speed (small fluctuations due to noise or interactions do not alter the results). The initial direction of motion for each particle at the beginning of each cycle is defined by the net repulsive force from the neighbors. If the initial direction were chosen randomly, particles would not form any stable structure. These findings provide a hint on the mechanism of lattice formation. Upon the system activation, particles start to experience repulsion from the neighbors (due to a field-induced polarization) and roll away from dense clusters. A temporal cessation of the activity and subsequent reenergizing of the system leads to rapid reorientation of particles' velocities against the local density gradients and results in a reciprocating motion of particles between the two sets of lattices.

In order to gain additional insights into the observed self-organization, we explore the response of the system to changes in the pulse duration τ_{on} and distance between the pulses τ_{off}, see Fig. 2(a) and Video S3 in the Supplemental Material [38]. The lower limit of $\tau_{on} \approx 20$ ms for the lattices phase comes from a minimum time and distance rollers must travel to interact with each other as well as to overcome the intrinsic positional noise in the system. This limit naturally depends on the particles' density and may be significantly longer for low densities as discussed

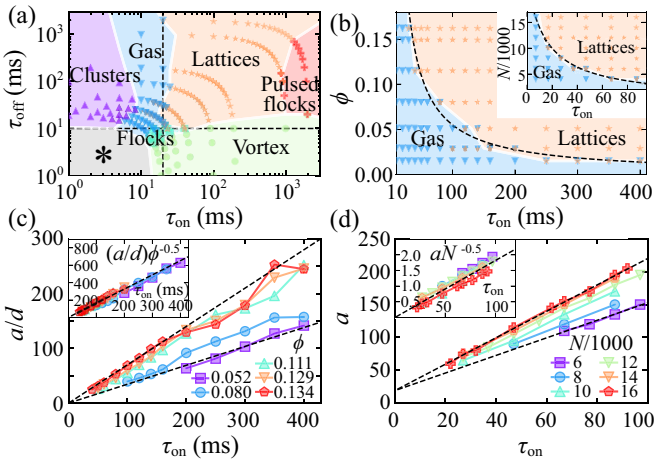

FIG. 2. (a) Dynamic phases formed by rollers for different τ_{on} and τ_{off}. $\phi = 0.120$, $E = 2.7$ V μm^{-1}. The system is confined by a cylindrical well with a diameter $D = 1$ cm. The phases marked as "$*$" have been previously reported in Ref. [6]. See Video S3 in the Supplemental Material [38] for more details. (b) Lattices and gas formed at different τ_{on} and ϕ ($\tau_{off} \geq 40$ ms). The dashed line is a fit of the boundary between phases by a function $\phi = A/\tau_{on}$, see text for details. Inset: dynamic phase diagram obtained from simulations. N is the number of particles in the system. (c),(d) Dependence of the lattice constant on τ_{on} for different area fractions in (c) experiments and (d) simulations. $D = 1.5$ mm. The dashed lines are linear fits for the lowest and highest area fractions. Insets in (c) and (d), experimental and simulation data with the lattice constant rescaled by a $\sqrt{\phi}$.

below. For $\tau_{on} > 1$ s, the particles' velocities at the end of each cycle become uncorrelated with initial orientations and, therefore, rollers are not able to alternate between fixed stable patterns. The vortex phase in Fig. 2(a) corresponds to the formation of a continuous single vortex at $\tau_{off} < 10$ ms. At this phase, the termination of energy injection is so brief that particles do not fully stop. In the pulsed flocks phase, the formation of the global vortex is interrupted every period of the signal. At small τ_{on}, rollers' dynamics resembles a gas motion with a tendency to form clusters as τ_{on} further decreases, see Fig. 2(a). The lattices can be distinguished from the gas by periodic oscillations of the density profile, see Figs. S4 and S6 in [38]. The crossover between those two dynamic states is continuous and smooth (see Fig. S4 [38]). Complex behavior of the system at small τ_{off} and τ_{on} [marked gray in Fig. 2(a)] corresponds to rollers with incomplete depolarization studied in [6].

Similar to other active systems, the formation of globally correlated states (like lattices) can only be observed at particle densities above a certain threshold. We investigate in experiment and simulations the behavior of the critical particle number density, necessary to facilitate the formation of lattices, as a function of the run time τ_{on}. This transition is accessible only at τ_{off} and τ_{on} time larger than the polarization relaxation time τ_{MW}. At low densities, particles need longer time to reach and interact with the neighbors, and as a result, a longer run time is required to support the dynamic lattice. Correspondingly, as the density of the rollers increases, the minimum run time to form the lattice decreases, see Fig. 2(b). The boundary between the gas and lattices follows a simple relation connecting the particle number density ϕ and the run time τ_{on}: $\phi = A/\tau_{on}$. The above scaling is valid for the whole range of scanned parameters ($10 < \tau_{on} < 400$ ms and $0.015 < \phi < 0.17$), and A here is a constant that depends on the properties of the system (particle size, activity, and liquid media). $A = 5.5$ ms for our experimental systems.

The lattice constant a grows with τ_{on}, see Fig. 2(c). Nevertheless, all the lines obtained at different densities collapse into a single line when rescaled by a $\sqrt{\phi}$, see Fig. 2(c) inset. Such scaling possibly comes from the similarity of the lattice density profiles at different ϕ that scale with the size of the unit cell, see Fig. S12 in [38]. Correspondingly, the evolution of the lattice constant a with the run time τ_{on} can be written as $a = kd\tau_{on}\sqrt{\phi}$, where k is the system-dependent constant, the slope of the rescaled line ($k = 1.63$ ms^{-1} for our system). The simulation results capture the similar trend, see Fig. 2(d). The above scalings can be used to estimate a number of particles per unit cell of the lattice at the transition point between the gas and lattice phases. As the particles' distribution over the system is homogeneous, the number of particles per unit cell of the square lattice can be estimated as $n = 4a^2\phi/(\pi d^2)$. Substituting a and ϕ by its dependence

on τ_{on} at the transition boundary between the gas and lattice phases, one obtains that the number of rollers per unit cell at the transition is $n_c = 4k^2A^2/\pi$ (see more details in Supplemental Material, Note S2) [38]. Since n_c is ϕ and τ_{on} independent, the number of particles per unit cell is the same at any transition point between the gas and lattice phases [the dashed line in Fig. 2(b)] regardless of the size of the unit cell.

The dynamic square lattices do not have an ideal order at macroscopic distances and often develop a number of defects, see Fig. S2 in [38]. To characterize the order of self-organized lattices, we calculate the local degree of fourfold symmetry for each vertex j in a lattice: $\Psi_4 = 1/4|\sum_{k=1}^{4}\exp(4i\theta_k)|$, where θ_k are polar angles of four closest neighbors with the origin at j vertex. The probability distribution functions (PDFs) of Ψ_4 for stable lattices at different τ_{on} show peaks at $\Psi_4 = 1$, indicating a presence of a well-defined fourfold symmetry in the order, see Fig. 3. The peaks get suppressed with the increase of the run time τ_{on}, reflecting the emergence of imperfections due to fluctuations of particles' velocities and the development of a global collective motion (vortex). The formation of the local order may be further quantified by a time evolution of the order parameter $\langle\Psi_4\rangle$ defined as Ψ_4 averaged over the whole system, see Figs. 3(a) and 3(b), insets. The temporal evolution of $\langle\Psi_4\rangle$ suggests that dynamic lattices emerge within 100 cycles, however, they never become geometrically perfect as $\langle\Psi_4\rangle$ reaches the plateau ($\approx$0.8). The system does not fully anneal all the defects even after many thousands of activity cycles.

In Quincke rollers system, the mechanism of self-organization with two alternating complementary lattices regulated by a density gradient limits the types of stable lattices to square lattices for any combination of excitation field parameters, while granular vibrated systems often demonstrate transitions between stripes, square, and hexagonal lattices with a change of the driving parameters [31–34,41,42]. The fixed geometry of the lattices at a wide range of the driving field parameters enables the study of the collective memory effects [43] in the system. Ramping the control parameter τ_{on} up and down at a fixed rate reveals

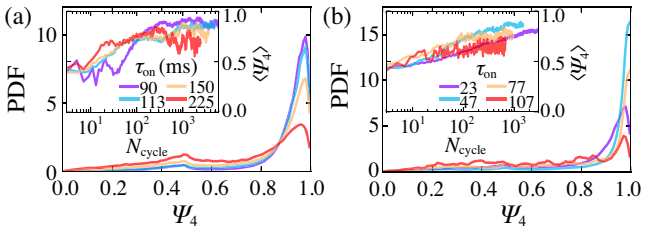

FIG. 3. Probability distribution functions of the local order parameters Ψ_4 in a stable lattice formed at different τ_{on} in (a) experiments and (b) simulations. Insets: temporal evolution of $\langle\Psi_4\rangle$. $E = 3.0\ \mathrm{V}\,\mu\mathrm{m}^{-1}$, $\tau_{on} = 112.5$ ms, $\tau_{off} = 12.5$ ms, $\phi = 0.114$, $D = 1$ cm. Also see Videos S4 and S5 in [38].

a dynamic hysteresis on a vs τ_{on}, see Figs. 4(a) and 4(b). The size of the hysteresis loop increases with the ramping rate. Interestingly, the lattices demonstrate asymmetry in the resistances against the expansion and compression stresses at a certain range of stresses, see Figs. 4(c) and 4(d). The lattices smoothly transition to smaller size unit cells if τ_{on} is decreased by 10%, but break down and reassemble into a larger lattices when τ_{on} is increased by the same amount. This is manifested by a temporal drop of the order parameter, see Fig. 4(d). If the relative change of τ_{on} is larger than 15%, then lattices prefer to completely disintegrate for both compression and expansion stresses. In addition, the response of the lattices to the compression occurs faster than to expansion if $\tau_{on} \leq 10\%$, see Fig. 4(c).

In conclusion, the temporal modulation of activity in the system of Quincke rollers provides a robust technique for accessing and controlling dynamic self-organized states that are not available upon continuous energy injection. A combination of experiments and numerical simulations has been used to investigate the physical mechanism that guides the formation of the reported patterns. A dominant role of electrostatic repulsion over hydrodynamic velocity alignment interactions immediately upon system reactivation results in a reciprocating motion of rollers between two stable square lattices. The lattices are reconfigurable with the control of the characteristic lattice constant by the

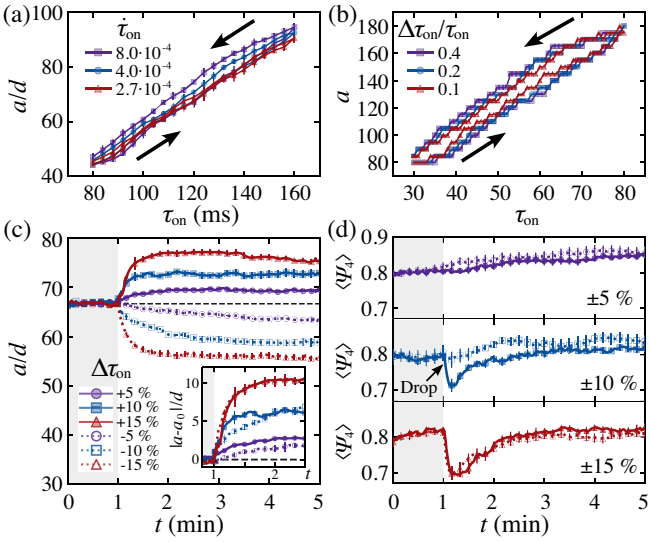

FIG. 4. Hysteresis loops for different ramping rates of τ_{on} in (a) experiments and (a) simulations. Arrows indicate the direction of the hysteresis loop. The starting point is $\tau_{on} = 80$ ms (experiments) and 30 (simulations). See also Videos S6 and S7 in [38]. (c),(d) The evolution of the (c) lattice constant and (d) the local order parameter $\langle\Psi_4\rangle$ of the square lattices in response to the increase (solid symbols) or decrease (open symbols) of the τ_{on} relative to the initial value of $\tau_{on} = 120$ ms. The data are averaged over five experimental realizations for each curve. Inset in (c) shows the absolute change of a compared to the initial value a_0.

particles' run time. The minimal number of particles per unit cell of the lattice required to facilitate the lattice formation is independent of the lattice constant and the average particle number density. Our results provide new insights into the collective behavior and control of active colloidal ensembles by means of a temporal modulation of activity. The reported mechanism should, in principle, be applicable to other active systems where the collective behavior is governed by the interplay of isotropic repulsion and hydrodynamic velocity alignment interactions.

The research was supported by the U.S. Department of Energy, Office of Science, Basic Energy Sciences, Materials Sciences and Engineering Division. Use of the Center for Nanoscale Materials, an Office of Science user facility, was supported by the U.S. Department of Energy, Office of Science, Office of Basic Energy Sciences, under Award No. DE-AC02-06CH11357.

*sokolov@anl.gov

[1] T. Sanchez, D. T. Chen, S. J. DeCamp, M. Heymann, and Z. Dogic, Nature (London) **491**, 431 (2012).
[2] A. Snezhko and I. S. Aranson, Nat. Mater. **10**, 698 (2011).
[3] J. Palacci, S. Sacanna, A. P. Steinberg, D. J. Pine, and P. M. Chaikin, Science **339**, 936 (2013).
[4] R. Bastien and P. Romanczuk, Sci. Adv. **6**, eaay0792 (2020).
[5] B. Zhang, A. Sokolov, and A. Snezhko, Nat. Commun. **11**, 4401 (2020).
[6] H. Karani, G. E. Pradillo, and P. M. Vlahovska, Phys. Rev. Lett. **123**, 208002 (2019).
[7] A. Sokolov, A. Mozaffari, R. Zhang, J. J. de Pablo, and A. Snezhko, Phys. Rev. X **9**, 031014 (2019).
[8] T. Vicsek and A. Zafeiris, Phys. Rep. **517**, 71 (2012).
[9] O. Feinerman, I. Pinkoviezky, A. Gelblum, E. Fonio, and N. S. Gov, Nat. Phys. **14**, 683 (2018).
[10] A. Cavagna and I. Giardina, Annu. Rev. Condens. Matter Phys. **5**, 183 (2014).
[11] F. A. Lavergne, H. Wendehenne, T. Bäuerle, and C. Bechinger, Science **364**, 70 (2019).
[12] A. Sokolov, I. S. Aranson, J. O. Kessler, and R. E. Goldstein, Phys. Rev. Lett. **98**, 158102 (2007).
[13] V. Gyrya, I. S. Aranson, L. V. Berlyand, and D. Karpeev, Bull. Math. Biol. **72**, 148 (2010).
[14] A. Sokolov and I. S. Aranson, Phys. Rev. Lett. **109**, 248109 (2012).
[15] M. C. Marchetti, J.-F. Joanny, S. Ramaswamy, T. B. Liverpool, J. Prost, M. Rao, and R. A. Simha, Rev. Mod. Phys. **85**, 1143 (2013).
[16] E. Lushi, H. Wioland, and R. E. Goldstein, Proc. Natl. Acad. Sci. U.S.A. **111**, 9733 (2014).
[17] D. Nishiguchi, I. S. Aranson, A. Snezhko, and A. Sokolov, Nat. Commun. **9**, 4486 (2018).
[18] A. E. Hamby, D. K. Vig, S. Safonova, and C. W. Wolgemuth, Sci. Adv. **4**, eaau0125 (2018).
[19] A. Bricard, J.-B. Caussin, N. Desreumaux, O. Dauchot, and D. Bartolo, Nature (London) **503**, 95 (2013).
[20] S. Sánchez, L. Soler, and J. Katuri, Angew. Chem. Int. Ed. **54**, 1414 (2015).
[21] S. J. Ebbens and D. A. Gregory, Acc. Chem. Res. **51**, 1931 (2018).
[22] K. Han, G. Kokot, S. Das, R. G. Winkler, G. Gompper, and A. Snezhko, Sci. Adv. **6**, eaaz8535 (2020).
[23] J. Zhang, R. Alert, J. Yan, N. S. Wingreen, and S. Granick, Nat. Phys. **17**, 961 (2021).
[24] T. Bäuerle, R. C. Löffler, and C. Bechinger, Nat. Commun. **11**, 2547 (2020).
[25] M. Driscoll, B. Delmotte, M. Youssef, S. Sacanna, A. Donev, and P. Chaikin, Nat. Phys. **13**, 375 (2017).
[26] J. Yan, M. Han, J. Zhang, C. Xu, E. Luijten, and S. Granick, Nat. Mater. **15**, 1095 (2016).
[27] A. Bricard, J.-B. Caussin, D. Das, C. Savoie, V. Chikkadi, K. Shitara, O. Chepizhko, F. Peruani, D. Saintillan, and D. Bartolo, Nat. Commun. **6**, 7470 (2015).
[28] Z. Zhang, H. Yuan, Y. Dou, M. O. de la Cruz, and K. J. Bishop, Phys. Rev. Lett. **126**, 258001 (2021).
[29] B. Zhang, H. Karani, P. M. Vlahovska, and A. Snezhko, Soft Matter **17**, 4818 (2021).
[30] B. Zhang, H. Yuan, A. Sokolov, M. O. de la Cruz, and A. Snezhko, Nat. Phys. (2021), 10.1038/s41567-021-01442-6.
[31] S. Douady, S. Fauve, and C. Laroche, Europhys. Lett. **8**, 621 (1989).
[32] S. Fauve, S. Douady, C. Laroche *et al.*, J. Phys. **50**, 5 (1989).
[33] P. B. Umbanhowar, F. Melo, and H. L. Swinney, Nature (London) **382**, 793 (1996).
[34] F. Melo, P. B. Umbanhowar, and H. L. Swinney, Phys. Rev. Lett. **75**, 3838 (1995).
[35] G. Quincke, Ann. Phys. (Berlin) **295**, 417 (1896).
[36] A. Tsebers, Fluid Dyn. **15**, 245 (1980).
[37] B. Zhang, B. Hilton, C. Short, A. Souslov, and A. Snezhko, Phys. Rev. Research **2**, 043225 (2020).
[38] See Supplemental Material at http://link.aps.org/supplemental/10.1103/PhysRevLett.128.018004 for additional figures, notes, and videos.
[39] D. Kagan, S. Balasubramanian, and J. Wang, Angew. Chem. **123**, 523 (2011).
[40] I. Buttinoni, J. Bialké, F. Kümmel, H. Löwen, C. Bechinger, and T. Speck, Phys. Rev. Lett. **110**, 238301 (2013).
[41] C. Bizon, M. D. Shattuck, J. B. Swift, W. D. McCormick, and H. L. Swinney, Phys. Rev. Lett. **80**, 57 (1998).
[42] I. S. Aranson and L. S. Tsimring, Rev. Mod. Phys. **78**, 641 (2006).
[43] I. D. Couzin, J. Krause, R. James, G. D. Ruxton, and N. R. Franks, J. Theor. Biol. **218**, 1 (2002).